agriculture

MDPI

Article

A Dual-Source Energy Balance Model Coupled with Jarvis Canopy Resistance for Estimating Surface Evapotranspiration in Arid and Semi-Arid Regions

Qiutong Zhang [1], Jinling Kong [1,*], Lizheng Wang [1], Xixuan Wang [1], Zaiyong Zhang [2], Yizhu Jiang [3] and Yanling Zhong [1]

[1] College of Geological Engineering and Geomatics, Chang'an University, Xi'an 710054, China; zqt_chd@chd.edu.cn (Q.Z.); 2021126059@chd.edu.cn (L.W.); xixuan_wang999@163.com (X.W.); 2019026021@chd.edu.cn (Y.Z.)
[2] College of Water and Environment, Chang'an University, Xi'an 710054, China; zaiyongzhang@126.com
[3] College of Earth Sciences and Resources, Chang'an University, Xi'an 710054, China; yzjiang@chd.edu.cn
* Correspondence: jlkong@163.com

Abstract: Soil moisture is one of the main factors influencing evapotranspiration (ET) under soil water stress conditions. The $\mathrm{TSEB_{SM}}$ model used soil moisture to constrain soil evaporation. However, the transpiration schemes constrained by soil moisture require greater physical realism and the soil evaporation schemes parameters usually need calibration. In this study, the $\mathrm{TSEB_{SM}}$ model was enhanced by incorporating Jarvis's canopy resistance which considered the influence of soil moisture on transpiration schemes. We assessed the new model ($\mathrm{TSEB_{SM+}}$) in the Heihe and Haihe basins of China. The $\mathrm{TSEB_{SM+}}$ model displayed a consistency to the TSEB in the ET estimation at the A'rou site, but approximately 30% and 35% reductions in RMSEs at the Huazhaizi and Huailai sites. It produced approximately 20% and 10% of the reductions in the ET RMSEs at the Huailai and A'rou sites compared to the $\mathrm{TSEB_{SM}}$ model, but had a similar performance at the Huazhaizi site. Moreover, the $\mathrm{TSEB_{SM+}}$ model estimated ET in the Heihe River Basin with an RMSE of 0.58 $\mathrm{mm \cdot day^{-1}}$, and it was sensitive to the soil moisture, particularly when the soil moisture was below 30%. In conjunction to soil moisture, the $\mathrm{TSEB_{SM+}}$ model could potentially be a more effective tool for monitoring the ET.

Keywords: evapotranspiration; soil water stress; TSEB; canopy resistance

check for updates

Citation: Zhang, Q.; Kong, J.; Wang, L.; Wang, X.; Zhang, Z.; Jiang, Y.; Zhong, Y. A Dual-Source Energy Balance Model Coupled with Jarvis Canopy Resistance for Estimating Surface Evapotranspiration in Arid and Semi-Arid Regions. *Agriculture* **2024**, *14*, 2362. https://doi.org/10.3390/agriculture14122362

Academic Editor: Alexander Gröngröft

Received: 19 September 2024
Revised: 19 December 2024
Accepted: 20 December 2024
Published: 22 December 2024

Copyright: © 2024 by the authors. Licensee MDPI, Basel, Switzerland. This article is an open access article distributed under the terms and conditions of the Creative Commons Attribution (CC BY) license (https://creativecommons.org/licenses/by/4.0/).

1. Introduction

Evapotranspiration (ET), which includes soil evaporation (E) and plant transpiration (T), is an essential part of the global water cycle and a vital connection between the surface energy, carbon, and water on land [1,2]. About 60% of the global annual mean precipitation returns to the atmospheric system in the form of ET, and more than half of the surface-available energy is released in the form of ET [3,4], especially in arid and semi-arid regions, where the proportion has reached 90% [5]. Therefore, accurately estimating the ET distribution at the temporal and spatial scales is highly significant for studies on climate, hydrology, drought monitoring, especially for crop yield prediction [6].

Remote sensing (RS) observations can provide information on land surfaces in connection with the water and energy fluxes across broad regions at multiple scales, which makes it possible to apply traditional hydrologic ET estimation methods at the regional and global scales [7]. Compared to traditional ET point measurements, RS-based algorithms have been recognized as an effective way to derive the ET across an extensive range at the temporal and spatial scales over the last few decades [8], and many RS-based methods have been developed to quantify the ET and surface fluxes using remotely sensed data. According to their different mechanisms, the methods can be classified into temperature–vegetation index characteristic space methods [9,10], surface energy balance (SEB) models [11,12], traditional ET approaches combined with remotely sensed data [13,14], and data-driven methods [15–20]. The SEB model, which searches for an optimal compromise between the parameters derived from physical observations without a lot of data inputs and those derived from the energy balance equation, is an especially prevalent method used to estimate the ET through remotely sensed data, including the radiometric surface temperature, soil moisture (SM), and vegetation cover, at the regional and global scales [21,22].

The Two-Source Energy Balance (TSEB) model [12] and its revisions [23–25] partition the ET into E and T to overcome the limitations of the large-leaf model assumed by the single-source energy balance model [11,26], and it is more reliable than models that rely on a single source when applied to complicated and complex landcover and climatic conditions [21,27]. This model utilizes the radiometric surface temperature as a crucial boundary condition for the accurate calculation of the daytime sensible and latent heat fluxes of the soil and canopy components for land surfaces that are partially covered with vegetation. In the TSEB model, the latent heat flux (LE) of the plant transpiration is approximated via the Priestley–Taylor (PT) approach, and then the observation of the composite radiometric temperature is used to separate the temperatures of the canopy and soil components by a simple linear unmixing method. Finally, the energy conservation principle is used to infer the E and T. The TSEB model is useful for estimating the ET in various landscapes [28,29], and is superior to other thermal-based models [30,31]. However, previous studies have shown that the sensible heat flux (H) and LE are related to the soil moisture under water stress conditions, which causes the TSEB model to overestimate the ET [32–34]. Kustas et al. [35], Li et al. [36] and Feng et al. [37] recommend that reasonable vegetation inputs and the proper parameterization of the soil resistance or heat transfer resistance used in the original TSEB model can lead to reliable results for semiarid regions. However, we still do not fully comprehend the requirement for radiometric surface temperature measurements, which cannot be obtained under cloudy conditions and the estimation of the continuous daily ET from instantaneous values [38].

Soil moisture is one of the main factors affecting the ET [39] under water stress conditions, and SM fluctuations are significantly correlated with the ET [40]. Many researchers have introduced the SM as a limiting factor in RS-based evapotranspiration models (e.g., SEBS [41], PT [13,42] and PM [15,43]). Kustas et al. [38,44,45] developed an alternate form of the TSEB model named the $\mathrm{TSEB}_{\mathrm{SM}}$ model, in which passive microwave observations of soil moisture for the soil surface are used to replace the radiometric surface temperature. This new model applies a constraint on the soil evaporation using soil moisture data according to two coefficients that depend on the soil texture [46]. Li et al. [47] compared the $\mathrm{TSEB}_{\mathrm{SM}}$ model with the original TSEB model and found that the former performed better under medium vegetation cover and water-stressed conditions. However, the PT coefficient α_{PT} cannot be easily adjusted to accommodate a range of environmental conditions in these models [48], and larger differences are produced in the measured fluxes for dense vegetation cover conditions [47]. Because plant transpiration is frequently the dominant form of ET, it is important to consider the soil moisture constraint on the plant transpiration. The transpiration of the TSEB model may be more tightly constrained if the soil moisture and radiometric surface temperature are combined with the transpiration schema [49–51]. Therefore, the focus of many studies has been on the modification of PT formulation and its α_{PT} coefficient based on soil moisture in the TSEB model. Ait Hssaine et al. [49,52,53] developed an innovative calibration approach in which radiometric surface temperature, SM, and vegetation cover are used to determine the soil resistance and α_{PT} parameters for soil evaporation and plant transpiration. Zhuang et al. [54] used plant moisture and temperature constraints which depend on the PT-JPL model [13], to obtain a better canopy latent heat flux. Song et al. [50,51] and Tao et al. [55] used the PT formulation to calculate the E and T simultaneously, and coupled the soil moisture to calculate the temperatures of the soil and canopy components and the LE in a variety of plant cover and surface soil moisture situations. Nevertheless, the drawbacks still exist under dry and water deficient conditions [49].

Canopy resistance plays a key role in plant transpiration, constraining the transfer of root zone water to vapor [15]. In order to describe plant transpiration using a more physically realistic model, the canopy conductance (Gc) has been widely used to estimate the ET in many RS-based Penman–Monteith (PM) models [14,43]. Gan et al. [48,56] and Bu et al. [57] used the canopy conductance model instead of the PT formulation in the original TSEB model to estimate the plant transpiration, and established a complete resistance network to estimate the ET. However, the influence of soil moisture on canopy conductance is not considered in these methods when establishing the canopy resistance. Previous studies have shown that the stomatal conductance decreases with a decrease in soil moisture [58]. Moreover, plant transpiration is usually dominant in the ET in dense vegetation cover conditions, and is therefore used to obtain more accurate ET estimations when the influence of soil moisture on the canopy conductance under water stress conditions is considered in arid and semi-arid regions.

In this study, the Jarvis canopy resistance model [59,60], in which the soil water stress is considered, was coupled to the $TSEB_{SM}$ model instead of the PT formulation in the original model (denoted as the $TSEB_{SM+}$ model) to compensate for the effect of soil moisture on vegetation transpiration under soil water stress in arid and semi-arid regions. The unknown soil surface resistance (r_{ss}) and canopy resistance (r_c) parameters in the $TSEB_{SM+}$ model were fitted using in situ measurement flux data. We used the $TSEB_{SM+}$ model to calculate the energy fluxes and ET at three sites with different soil moisture and vegetation covers under water-limited conditions, and we assessed the new model using half-hour EC flux data and the predictions from the $TSEB_{SM}$ and TSEB models as references. In addition, we estimated the ET and latent heat fluxes over the time series via the $TSEB_{SM+}$ model and compared them with the measured values. In addition, the model was also verified at the Heihe River Basin. Finally, we analyzed the sensitivity of the $TSEB_{SM+}$ model to soil moisture according to its performance for various soil moisture levels.

2. Materials and Methods

2.1. Study Areas and Datasets

To run the models and evaluate their performances, meteorological and surface heat flux measurements from three flux towers over Huazhaizi (2019–2021), Huailai (2019–2021), and A′rou (2019–2021) were chosen according to different underlying surface, vegetation coverage, and soil moisture levels. The Huazhaizi and A′rou sites are located in the Heihe River Basin of China and have a temperate continental climate, and the Huailai site is located in the Hai River Basin of China and has a temperate monsoon climate (Figure 1). Detailed descriptions of the three sites are presented in Table 1.

The landcover of the Huazhaizi site is desert steppe with a heterogeneous sparse/low grass distribution, and that of the A′rou site is cold grassland with a dense and homogeneous distribution. The landcover at Huailai Station is maize, which ran throughout the entire maize growing period during the study period. The three sites are located in an area with little annual precipitation and large potential evaporation, and the soil moisture is often unsaturated for most of the year.

We collected the in situ measurement data of the three sites, which included the observations of the automatic weather station and eddy covariance system (Table 2). The datasets for the Huailai site came from the multi-scale surface flux and meteorological element observation dataset for the Hai River Basin. The datasets for the Huazhaizi and A′rou sites came from the dataset for the Heihe integrated observatory network. Eddy covariance (EC) systems with a 10 Hz sampling frequency were utilized to measure the sensible (H) and latent (LE) heat fluxes which were mainly used for the model calibration and verification [61,62]. The ancillary meteorological observations, G and soil moisture were measured at the weather stations. In this paper, soil moisture measurements at a 4 cm depth were used to estimate the soil surface and canopy resistances. The in situ measurements were taken at 30 min intervals and either instantaneous measurements or an average of the measurements from 30 min before the specified observation time. According to the EC systems, the total LE and H were often lower than the available energy (Rn-G). Therefore, the Bowen ratio method was used to make closure modifications to the sensible and latent heat fluxes from the EC systems [63] before the flux measurements were used.

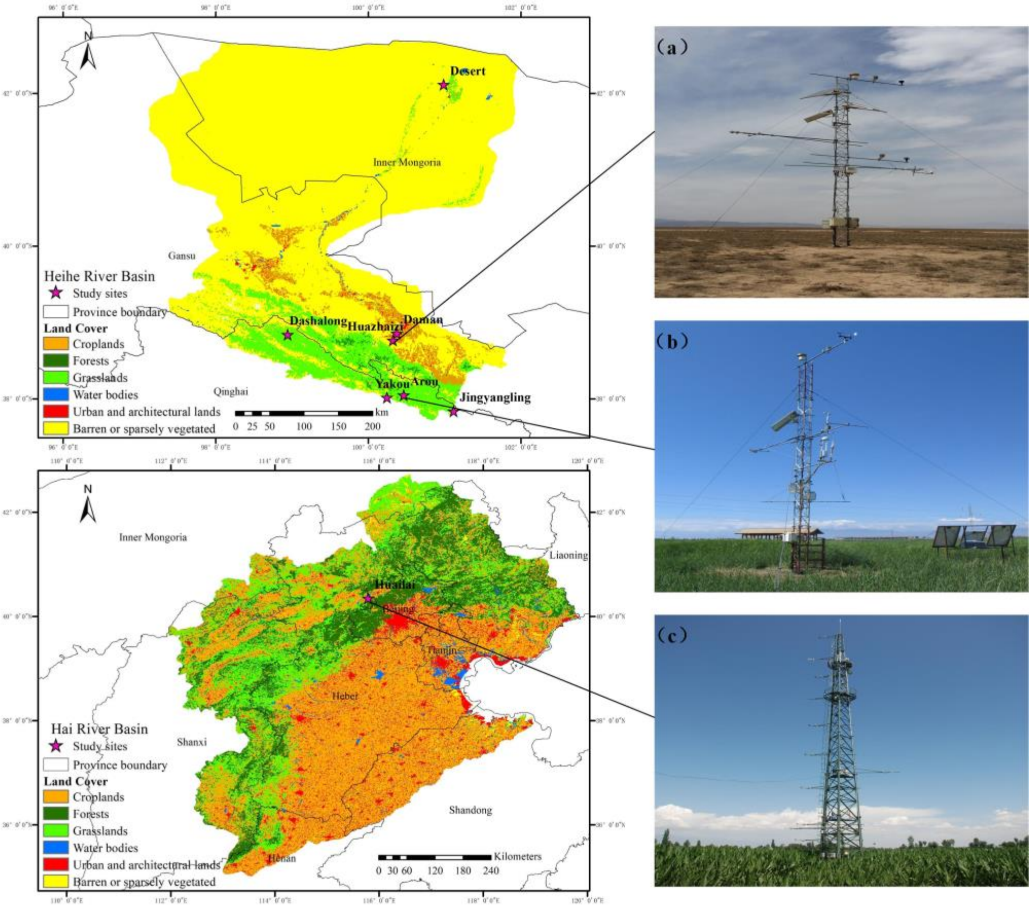

Figure 1. Maps of landcovers in Heihe and Haihe river basins and the locations of the EC flux towers ((**a**) the Huazhaizi site; (**b**) the A'rou site; (**c**) the Huailai site).

Table 1. Detailed descriptions of the sites used in this study.

Site	Huazhaizi	Huailai	A'rou
Study period	2019–2021	2019–2021	2019–2021
Latitude, longitude	100°19′12.36″ E, 38°45′57.24″ N	115°47′16.80″ E, 40° 20′ 56.76″ N	100°27′51.48″ E, 38°2′50.28″ N
Elevation	1731 m	480 m	3033 m
Annual precipitation	130 mm	392 mm	450 mm
Mean air temperature	7.3 °C	9.5 °C	1 °C
Land cover type	Desert steppe	Cold grassland	Maize
Mean soil moisture content [1]	13.27% (5.73–21.03%)	16.23% (12.03–26.25%)	34.20% (21.40–44.57%)

[1] Soil volumetric water content. The ranges of the soil water variation during the study period are shown in parentheses.

For each site, we selected the time from DOY 122 to DOY 274 every year when the vegetation was in the growing period and a half-hour scale from 8:00 to 17:00 for each day. All the records of good quality were selected for the simulations. In addition, we excluded the data when the LE, H, and $S_{\downarrow}$ were less than 0. The parameter-fitting dataset, which included the LAI, meteorological data, soil moisture, and energy flux observations, was taken from 2019 for the three sites. The validation dataset, which included the same types of inputs except for the observed fluxes, was from 2020 and 2021.

Table 2. Description of data for model validation at three sites.

Data	Measurement	Measuring Height	Resolution
Meteorological measurements	Air temperature (T_a)	5 m	10 min [1]
	Surface radiation temperature (T_{rad})	6 m	10 min [1]
	Specific humidity (RH)	5 m	10 min [1]
	Wind speed (u)	5 m/10 m [3]	10 min [1]
	Air pressure (p)	10 m	10 min [1]
	Precipitation (Rain)	10 m	10 min [1]
	Incoming radiation ($L_\downarrow/S_\downarrow$)	5 m/6 m [3]	10 min [1]
Subsurface measurements	Soil moisture (SM)	−2 cm/−4 cm/−10 cm	10 min [1]
	Soil temperature (T_s)	−2 cm/−4 cm/−10 cm	10 min [1]
Flux measurements	Soil heat flux (G)	−6 cm	30 min [1]
	Sensible heat flux (H)	5 m	30 min [1]
	Latent heat flux (LE)	5 m	30 min [1]
Remote sensing data	GLASS products (LAI)	-	500 m [2]/8 days [1]

[1] Temporal resolution. [2] Spatial resolution. [3] The measurement heights for the wind speed and incoming radiation at the Huazhaizi and A'rou sites were 5 m and 6 m, respectively, and those at the Huailai site were 10 m and 5 m, respectively.

We also collected the in situ measurement data of the automatic weather station and eddy covariance system for the Jingyangling, Yakou, Dashalong, Daman and Desert sites from 2019 to 2020, which have a similar landcover type to that of the A'rou site, while the Daman site has a landcover type that is similar to that of the Huailai site, and the Desert site has a landcover type that is similar to that of the Huazhaizi site. These data were used to verify the model's performance at the regional scale together with the Huazhaizi and A'rou sites.

We also needed the meteorological data, surface radiometric temperature, LAI, and SM of the Heihe River Basin to generalize the model to the regional scale. We collected the GLASS (Global Land Surface Satellite) LAI products with a temporal resolution of 8 days and spatial resolution of 1 km (http://www.glass.umd.edu/LAI/, accessed on 19 December 2024). The meteorological data were produced by using the Weather Research and Forecasting (WRF) model over the Heihe River Basin hourly with a spatial resolution of 0.05° [64], which needed to be downscaled to a 1 km spatial resolution. A machine learning based method was developed to generate a global spatiotemporal continuous surface soil moisture dataset with a 1 km resolution based on the ESA Climate Change Initiative (ESA-CCI) dataset [65]. The Western China daily 1 km spatial resolution all-weather land surface temperature dataset was collected to provide the surface radiometric temperature [66]. The SM, meteorological data, and surface radiometric temperature datasets are all from the Central Tibetan Plateau Data Center (https://www.tpdc.ac.cn/en/, accessed on 19 December 2024).

2.2. Enhanced Two-Source Energy Balance Model ($TSEB_{SM+}$)

The TSEB model [12] often overestimates the ET under soil moisture-stressed conditions and the input parameter (radiometric surface temperature) often cannot be obtained under cloudy conditions [32–34,38]. Kustas et al. [38,44,45] modified the TSEB model using the surface soil moisture derived from passive microwave sensors instead of the radiometric surface temperature to estimate the latent heat flux of the soil. In practice, the new $TSEB_{SM}$ model has the same energy balance for the canopy and soil as that of the original TSEB model

$$R_n = R_{ns} + R_{nc} \tag{1}$$

$$R_{ns} = H_s + LE_s + G \tag{2}$$

$$R_{nc} = H_c + LE_c \tag{3}$$

where H is the sensible heat flux, LE is the latent heat flux, R_n is the net radiation, and G is the soil heat flux (all in W·m^{-2}). The components of the soil and canopy are denoted by the subscripts s and c, respectively. G can be parameterized as a fraction of R_{ns} and expressed as the function $G = c_G R_{ns}$, where c_G is an empirical coefficient that remains unchanged for several hours during solar noon [67].

However, the soil evaporation is now explicitly represented as a function of the soil moisture via a soil resistance term, and the formulation for LE_s is expressed as follows:

$$LE_s = \frac{\rho C_p}{\gamma} \frac{h_r e(T_s) - e_a}{r_a + r_s + r_{ss}} \tag{4}$$

$$H_s = \rho C_p \frac{T_s - T_a}{r_a + r_s} \tag{5}$$

where ρ is the air density (kg·m^{-3}); C_p is the specific heat of the air (J·kg^{-1}·K^{-1}); γ is the psychrometric constant (0.667 hPa·K^{-1}); h_r is the relative humidity of the air adjacent to the soil moisture which can be computed via the surface soil moisture content [68]; T_a and T_s are the temperature of the air at the reference height and the soil temperature (K), respectively; e_a is the air vapor pressure (hPa); $e\ (T_s)$ is the saturated vapor pressure at temperature T_s (hPa); r_a is the aerodynamic resistance to the turbulent heat transport between the height of the canopy source (s·m^{-1}); r_s is the resistance to heat flow in the boundary layer immediately above the soil surface (s·m^{-1}) [8,35]; r_{ss} is the surface soil resistance to latent heat transfer and can be estimated using an exponential function of the soil moisture at the surface (s·m^{-1}):

$$r_{ss} = \exp\left(b_0 - b_1 \frac{SM}{SM_s}\right) \tag{6}$$

where b_0 and b_1 are the empirical coefficients that were given 8.2 and 4.3 in earlier studies [38] and were refitted in this study; the SM is the soil moisture content of the near surface and SM_s is the saturated soil moisture content (%). When the soil moisture is saturated, the soil surface is the evaporating surface and the water vapor is directly transported between it and the air through turbulence, which is mainly governed by aerodynamic resistance. When the soil moisture is unsaturated, the evaporating surface is below the soil surface and the diffusion of water vapor is hindered by the capillary action of the soil pores, which manifests as soil surface resistance and is related to the soil texture and moisture.

In the TSEB$_{\mathrm{SM}}$ model, the PT formulation is used to estimate the plant transpiration, which cannot be adapted to the change in transpiration under different soil moisture conditions. The parameter α_{PT} could not be described with a constant value under large diurnal variation in a vapor pressure deficit in semiarid and arid regions [69]. Therefore, we used the canopy resistance model related to soil moisture to replace the PT formulation and built the new TSEB$_{\mathrm{SM+}}$ model to estimate the LE of the canopy to simulate the evapotranspiration under soil water stress in dry regions. The LE_c formulation is expressed as follows:

$$LE_c = \frac{\rho C_p}{\gamma} \frac{e_s(T_c) - e_a}{r_a + r_c} \tag{7}$$

$$H_c = \rho C_p \frac{T_c - T_a}{r_a + r_x} \tag{8}$$

where T_c is the canopy temperature (K); $e_s\ (T_c)$ is the saturated vapor pressure at temperature T_c (hPa); r_x is the total boundary layer resistance of the complete canopy leaves (s·m^{-1}); r_c is the canopy resistance which can be expressed via the Jarvis canopy resistance model, which considers various environmental factors (s·m^{-1}), such as the T_a, vapor pressure deficit (D, kPa), R_n, and water stress of the root zone (SM, %). The Jarvis canopy resistance model is an empirical multi-factorial approach that includes the effective leaf area index (LAI_a) and meteorological factors, in which the soil moisture is also considered [59,70,71]:

$$r_c = \frac{r_{min}}{LAI_a f(R_n) f(D) f(T_a) f(SM)} \tag{9}$$

$$LAI_a = LAI/(0.3LAI + 1.2) \tag{10}$$

where LAI is the leaf area index; r_{min} is the minimum stomatal resistance; $f(R_n), f(D), f(T_a)$ and $f(SM)$ are the weighting functions that show the influence of the R_n, D, T_a, and SM on the plant, respectively.

$$f(R_n) = 1 - \exp(-R_n/a_1) \tag{11}$$

$$f(D) = 1 - a_2 D \tag{12}$$

$$f(T_a) = 1 - a_3(25 - T_a)^2 \tag{13}$$

$$f(\mathrm{SM}) = \left(\frac{SM - SM_r}{SM_s - SM_r}\right)^{a_4} \tag{14}$$

where SM_s and SM_r are the saturated and wilting soil moistures which are determined by the soil properties, and a_1, a_2, a_3 and a_4 are the empirical parameters and can be calibrated via the measured surface fluxes.

We first set the initial T_s and T_c and obtained the initial net radiative fluxes of the soil and canopy (R_{ns} and R_{nc}, respectively). Then, the new T_s and T_c were calculated by solving the corresponding energy balance equation using the Newton-Raphson iteration approach. We repeated the iterative procedures using the updated T_s and T_c, and the final T_s and T_c results were obtained when they had stable values (the difference between the two iterations was less than 0.1 K). The energy fluxes were derived after the T_s and T_c were obtained.

2.3. The Evaluation Metrics

We used the Mean Bias Error (*BIAS*), Root Mean Squared Error (*RMSE*), Wilmott Adjustment Index (WAI) and Coefficient of Determination (R^2) as the error metrics to evaluate the $\mathrm{TSEB_{SM+}}$ model, which are defined as follows:

$$BIAS = \sum_{i=1}^{N} (sim_i - obs_i)/N \tag{15}$$

$$RMSE = \sqrt{\sum_{i=1}^{N} (sim_i - obs_i)^2 / N} \tag{16}$$

$$\mathrm{WAI} = 1 - \frac{\sum_{i=1}^{N} (sim_i - obs_i)^2}{\sum_{i=1}^{N} \left(\left|sim_i - \overline{obs}\right| + \left|obs_i - \overline{obs}\right|\right)^2} \tag{17}$$

$$R^2 = 1 - \frac{\sum_{i=1}^{N} (sim_i - obs_i)^2}{\sum_{i=1}^{N} \left(obs_i - \overline{obs}\right)^2} \tag{18}$$

where *sim* and *obs* are the mean simulated and observed values, respectively, and N is the number of data points. The Bias provides the magnitude of the deviation of the simulated value from the measured value, the RMSE reflects the deviation of the actual difference between the simulated and observed values. The WAI and R^2 indicate the goodness of fit between the simulated and observed values of the model. Better estimations are produced when the RMSE value is smaller, the Bias value is closer to 0, and the WAI and R^2 values are closer to 1.

3. Results

3.1. Parameter Fitting and Validation

The parameter values are different under varying underlying surface and soil properties in the $\text{TSEB}_{\text{SM+}}$ model and should be fitted for each site. In this study, the sum of the RMSEs for the H and LE estimations were used as the penalty function, and the unknown parameters were optimized via the simulated annealing method. Considering that a single fit could cause contingencies for unknown parameters in the model, the parameter fitting procedure was repeated more than 20 times, and we chose the best one as the final result. Moreover, the parameters of the TSEB_{SM} model fitted according to the same method.

According to the results of the parameter fitting (Table 3), the R_n, D and SM had a considerable influence on the canopy resistance in the $\text{TSEB}_{\text{SM+}}$ model. The a_2 and a_3 coefficients have similar values for the three sites, which means that the D and T had an approximate effect on the canopy resistance at the different sites. However, there is a substantial difference in the a_1 and a_4 coefficients for the different sites. The canopy resistance was most affected by the SM at the Huazhaizi site and by the Rn at A'rou site, which could be related to the vegetation type, SM, and meteorological conditions at the different sites. In the TSEB_{SM} model, the more severe the soil water stress, the smaller the α_{PT} value. The b_0 and b_1 parameters, which are related to the soil surface resistance, are different from those of previous studies, which have values of 8.2 and 4.3 [46] for the TSEB_{SM} model and change according to the soil types.

Table 3. Parameter fitting via EC measurements in the $\text{TSEB}_{\text{SM+}}$ and TSEB_{SM} models at the three sites.

Model	**Site**	α_{PT}	a_1	a_2	a_3	a_4	b_0	b_1
$\text{TSEB}_{\text{SM+}}$	Huazhaizi	-	90.42	0.23	0.0027	2.13	8.86	3.33
	Huailai	-	516.52	0.19	0.0026	0.37	10.04	5.56
	A'rou	-	987.03	0.25	0.0025	0.45	8.34	3.21
TSEB_{SM}	Huazhaizi	0.75	-	-	-	-	14.01	14.99
	Huailai	0.93	-	-	-	-	8.32	3.09
	A'rou	1.26	-	-	-	-	7.46	1.12

3.2. Validation of Instantaneous Flux Estimated from the Model

The optimal parameters obtained via the parameter fitting were used to estimate the fluxes and were evaluated via EC observations at the different sites. Here, the RMSE, Bias, WAI, and R^2 were used to quantify the performance of the model, and the flux estimations for the TSEB_{SM} and original TSEB models were also used as references.

As illustrated in Figures 2–4, the consistency of the estimated and measured fluxes from the $\text{TSEB}_{\text{SM+}}$ model was obviously better than that for the TSEB model for the Huazhaizi and Huailai sites. The RMSEs of the estimated LE and H were basically halved for the Huazhaizi site and decreased by about 24 $\text{W}\cdot\text{m}^{-2}$ and 42 $\text{W}\cdot\text{m}^{-2}$ for the Huailai site, respectively, and the WAI and R^2 also showed significant improvement. Moreover, the estimation of the H and LE via the TSEB model were severely underestimated and overestimated for both sites, which could be because the low soil moisture restrained the soil evaporation via the dry soil layer on the soil surface [72] at both the sites and affected the stomatal conductance of the canopy [73] at the Huailai site. The other is because the soil resistance term in the TSEB model was not appropriately parameterized for the sparse cover conditions at the Huazhaizi site, where the LAI was lower than 1 over the whole growing season. However, the TSEB model performed as well as the $\text{TSEB}_{\text{SM+}}$ model for the A'rou site, where there was higher cover and soil moisture, although the slight overestimation trend for the LE was still found under low soil moisture.

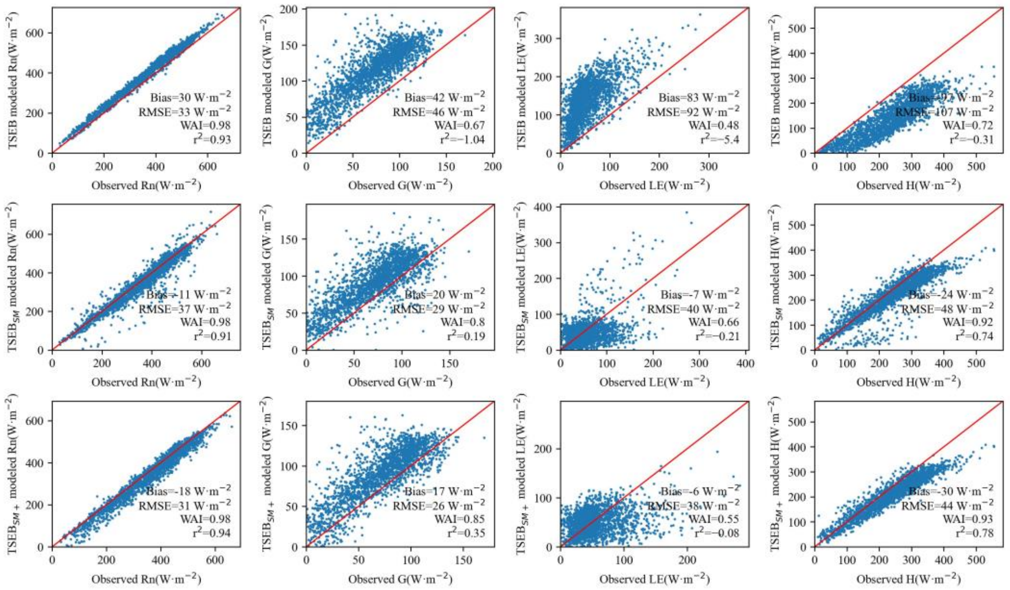

Figure 2. Scatterplots of estimated half-hour R_n, G, H and LE over the study period from the TSEB, TSEB$_{SM}$ and TSEB$_{SM+}$ models in comparison to the measurements from the EC system at the Huazhaizi site.

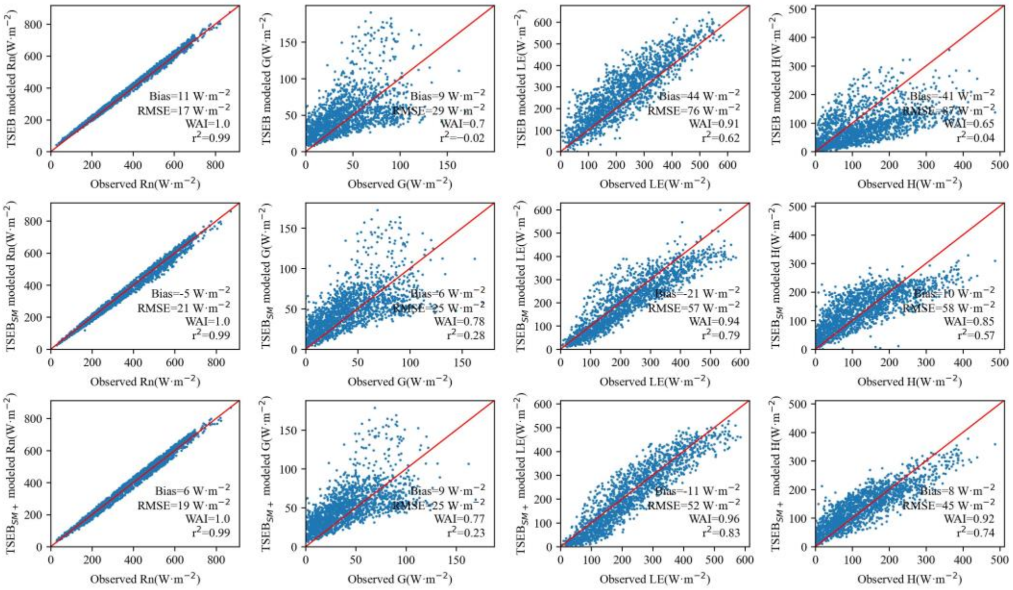

Figure 3. Scatterplots of estimated half-hour R_n, G, H and LE over the study period from the TSEB, TSEB$_{SM}$ and TSEB$_{SM+}$ models in comparison to the measurements from the EC system at the Huailai site.

The flux agreement between the estimations from the TSEB$_{SM}$ and TSEB$_{SM+}$ models and observed were appropriate during the study period for all the sites, but better performance was obtained from the TSEB$_{SM+}$ model for the Huailai and A'rou sites with high canopy cover conditions. The TSEB$_{SM+}$ model produced the LE with RMSEs of 52 W·m^{-2} and 44 W·m^{-2} versus 57 W·m^{-2} and 50 W·m^{-2} from TSEB$_{SM}$ model for the Huailai and A'rou sites, respectively, and the H RMSEs were 45 W·m^{-2} in place of 58 W·m^{-2} and 53 W·m^{-2} in place of 63 W·m^{-2} for both sites, respectively. The WAI and R^2 also improved, except for the R^2 in the H estimation at the A'rou site, which is likely because both models incorporate soil surface resistance, which is related to the soil moisture for the soil evaporation schemes, which is the main evapotranspiration component under the low vegetation cover condition for the Huazhaizi site. The difference in the fluxes between the estimations from the $TSEB_{SM}$ and $TSEB_{SM+}$ models and observed became larger as the soil moisture and LAI increased. The $TSEB_{SM+}$ model performed better than the $TSEB_{SM}$ model under high canopy cover conditions when they were used in arid and semi-arid regions with soil water stress.

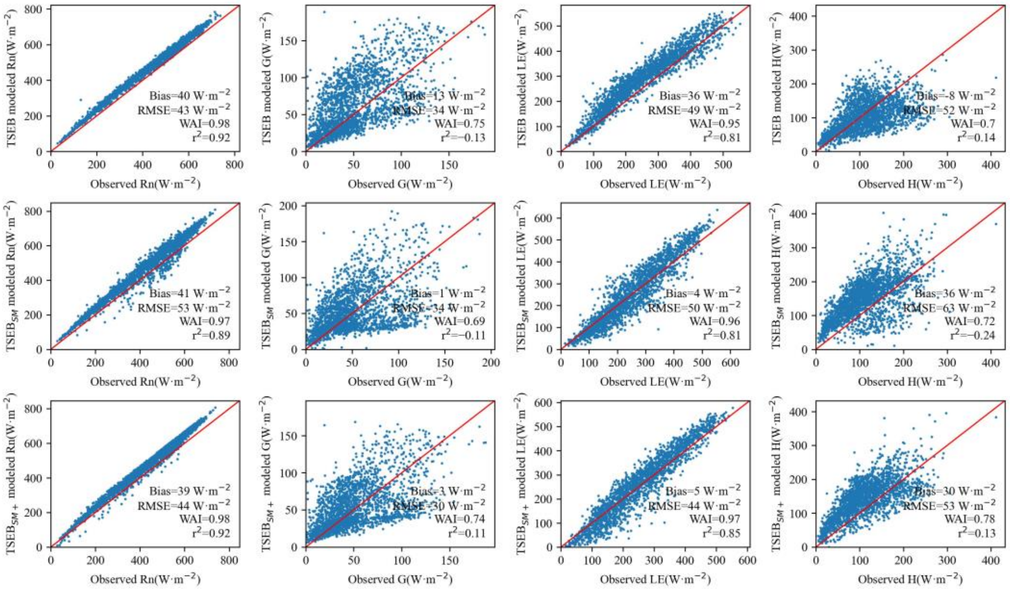

Figure 4. Scatterplots of estimated half-hour R_n, G, H and LE over the study period from the TSEB, $TSEB_{SM,}$ and $TSEB_{SM+}$ models in comparison to the measurements from the EC system at the A'rou site.

In addition, the accuracy of the G estimated via the $TSEB_{SM+}$ model was also improved for the three sites. The estimations of the G for the three models are slightly different even though the same method was used in them, which depended on the decomposition of the T_s. Moreover, the G, which was derived from three plates under the ground, had a very small geographic sample related to the heterogeneity of the landscape, which also caused the inconformity of the G from its estimated and measured values.

3.3. Validation of Daily ET Estimated from Model

Many applications connected to water can benefit from the LE at daylight scales and its daily fluctuations. We used the TSEB, $TSEB_{SM,}$ and $TSEB_{SM+}$ models to estimate the daily ET (actual evapotranspiration) from DOY122-274 for 2020 and evaluated it via the measured ET (Figures 5–7 and Table 4).

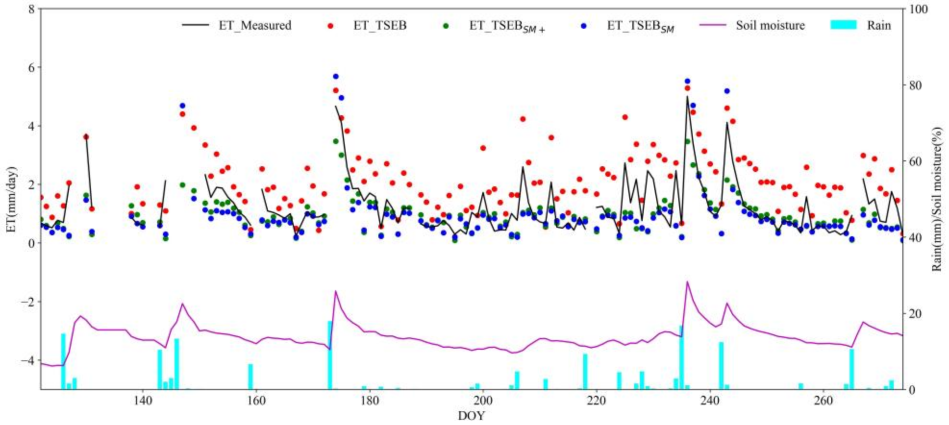

Figure 5. Comparison of daily ET between estimations via the TSEB, $TSEB_{SM,}$ and $TSEB_{SM+}$ models and observed from the EC system at the Huazhaizi site from DOY122-274 for 2020.

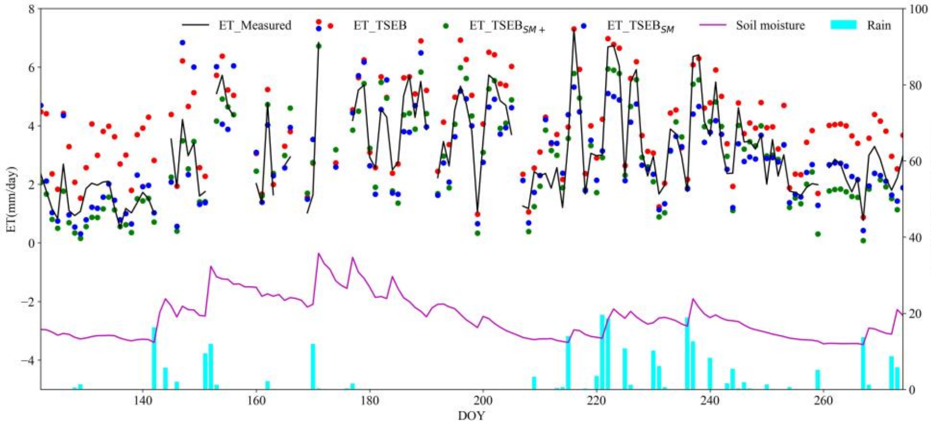

Figure 6. Comparison of daily ET between estimations via the TSEB, TSEB$_{SM,}$ and TSEB$_{SM+}$ models and observed from the EC system at the Huailai site from DOY122-274 for 2020.

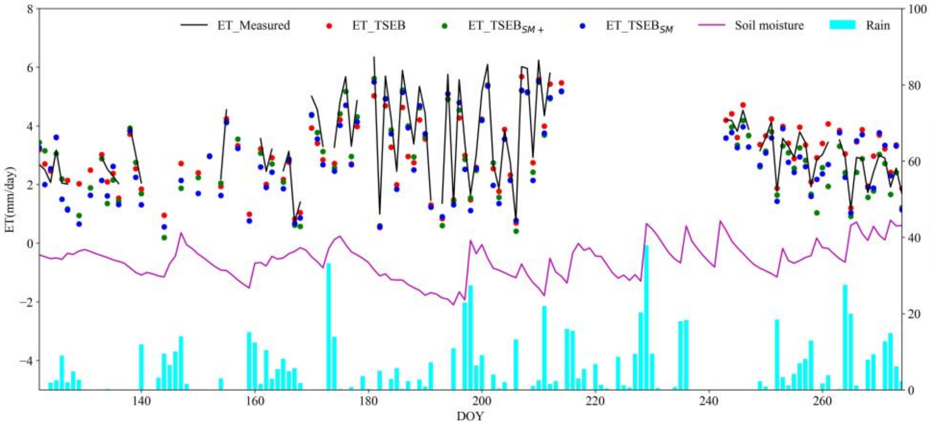

Figure 7. Comparison of daily ET between estimations via the TSEB, TSEB$_{SM,}$ and TSEB$_{SM+}$ models and observed from the EC system at the A′rou site from DOY122-274 for 2020.

Table 4. Errors between daily ET estimations via the TSEB, TSEB$_{SM,}$ and TSEB$_{SM+}$ models and the EC system measured at the Huazhaizi, Huailai and A′rou sites.

Models	**Sites**	**BIAS (mm·day^{-1})**	**RMSE (mm·day^{-1})**	**WAI**	**R^2**
TSEB	Huazhaizi	0.84	1	0.78	−0.17
	Huailai	0.88	1.12	0.87	0.48
	A′rou	−0.20	0.56	0.95	0.84
TSEB$_{SM}$	Huazhaizi	−0.30	0.68	0.87	0.46
	Huailai	−0.14	0.90	0.91	0.66
	A′rou	−0.47	0.62	0.94	0.80
TSEB$_{SM+}$	Huazhaizi	−0.31	0.69	0.79	0.43
	Huailai	−0.26	0.72	0.95	0.79
	A′rou	−0.44	0.56	0.96	0.83

There was low and constant daily ET during the study period for the Huazhaizi site, except after rain events, and the average ET was 1.24 mm·day^{-1} during DOY 122-274. For the Huailai and A′rou sites, the daily ET begins to gradually increase in early May (DOY 150) and then increases quickly along with the maize and grass growth, and then it gradually decreases beginning at the end of August (DOY 240), when the plants grow and enter the senescent period. The average ET values were 3.06 mm·day^{-1} and 3.28 mm·day^{-1} during DOY 122-274 for the Huailai and A′rou sites, respectively.

The TSEB model often overestimated the ET under water-limited conditions, especially for the Huazhaizi and Huailai sites, where the soil moisture is always lower than 30%. The RMSE between the observed and estimated ETs was more than 1 mm·day^{-1}. In addition, larger errors were always found for the study period for the Huazhaizi site. For the Huailai site, larger errors were found at the beginning and end of the study period, when the corn was in the sowing and ripening stage. When the corn was in the growing period, the error of the model was relatively small because plant transpiration from the TSEB$_{SM+}$ model was also improved when compared to those of the TSEB model. When the soil moisture increased, the soil and canopy resistance weakened, and a higher ET was estimated via the TSEB$_{SM+}$ model. For the A'rou site, the ET estimation via the TSEB and TSEB$_{SM+}$ models produced better results than the TSEB$_{SM}$ model, even though the ET estimate errors via the TSEB$_{SM}$ model were acceptable. In summary, the TSEB model is suitable for conditions of sufficient soil moisture and high vegetation coverage, while the TSEB$_{SM}$ model is suitable for conditions of soil moisture deficiency and sparse vegetation coverage. However, the TSEB$_{SM+}$ model could be adapted to the conditions of dry or moist soil surfaces and sparse or high vegetation coverage.

However, the TSEB$_{SM}$ and TSEB$_{SM+}$ models underestimated the ET after precipitation events. In addition, there were negative biases for the ET estimated via the TSEB$_{SM}$ and TSEB$_{SM+}$ models for the Huazhaizi and Huailai sites, which is likely because it is difficult to measure the amount of evaporation from plant intercepted water after precipitation events. In addition, these discrepancies due to the soil moisture decouple at different depths [72], and the soil surface energy balance is more closely correlated with the surface soil moisture conditions compared to deeper layers [32]. The three models were able to follow the annual ET dynamics recorded by the EC systems for the A'rou site; however, negative biases were found due to the frequent precipitation events.

3.4. Application of the Model at the Regional Scale

The TSEB$_{SM+}$ model had a distinct advantage for the estimation of the LE/ET under soil water stress conditions at the Huazhaizi, Huailai, and A'rou sites. To further verify the practical value of the TSEB$_{SM+}$ model, we used it to estimate the daily ET at the regional scale. The Heihe River Basin was chosen as the study area, because it is a typical arid and semi-arid area with a dry climate and scarce precipitation. The upstream region is predominantly alpine meadows, the midstream region mainly consists of artificial oases and irrigated land, and the downstream region is largely covered by the Gobi Desert, with the exception of a narrow band of riparian forests along the Heihe River.

We extracted the areas covered by alpine meadows, croplands with corn, and desert steppes in the Heihe River Basin, and the TSEB$_{SM+}$ model with fitted parameters for the three vegetation cover types was used to estimate the daily ET. Validation was performed using in situ measurements from the EC systems, for which the energy balance closure had already been applied at seven sites, including the Huazhaizi and A'rou sites. We selected 11 days from 2019 (DOY163, DOY185, DOY206, DOY212, DOY223 and DOY227) and 2020 (DOY183, DOY208, DOY214, DOY232, and DOY239) with favorable weather conditions and estimated the daily ET using the TSEB$_{SM+}$ model (Figure 8).

We compared the daily ET measured via the EC system with the estimation of the TSEB$_{SM+}$ model at seven sites (Figure 9) to verify the model's performance at the regional scale. The RMSE of the estimated daily ET is 0.62 mm·day^{-1} which is similar to the average performance of the model at the Huazhaizi, Huailai and A'rou sites, and the index of the WAI and R^2 is almost close to 1. We also statistically analyzed the model performance under the different landcover types separately, and the RMSEs of the estimated daily ET are 0.67 mm·day^{-1}, 0.50 mm·day^{-1} and 0.56 mm·day^{-1} for the alpine meadows, croplands, and desert steppes, respectively. The daily ET estimated via the TSEB$_{SM+}$ model is higher than the measured daily ET on alpine meadows and desert steppes, which is contrary to the results obtained at the A'rou and Huazhaizi sites. This is likely caused by the SM products, which are higher than the measured values for the alpine meadow and desert steppe regions. In general, the TSEB$_{SM+}$ model can be effectively applied to the estimation of the ET at the regional scale in arid and semi-arid regions.

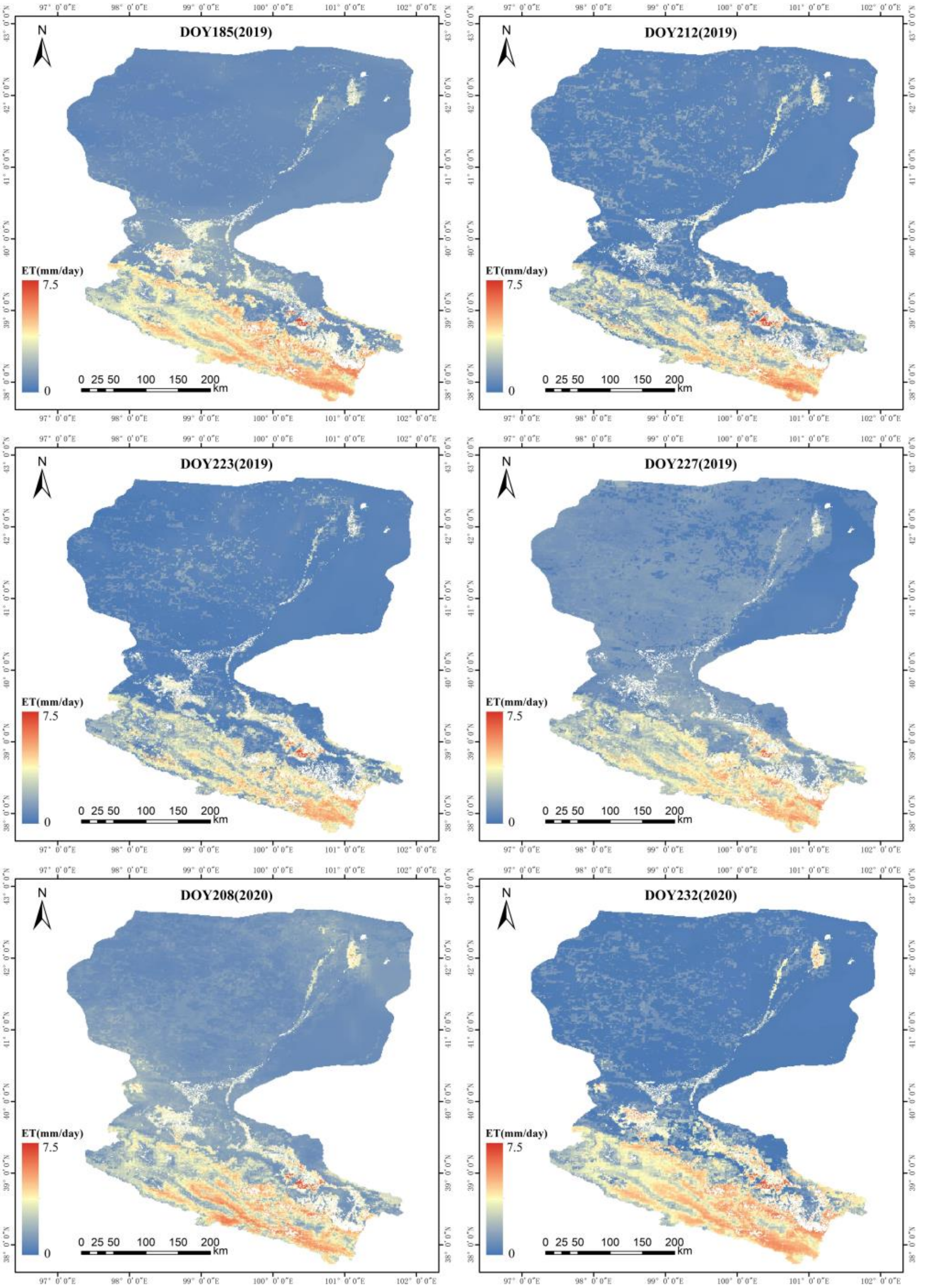

Figure 8. The daily ET estimated via the TSEB$_{SM+}$ model for alpine meadows, croplands with corn, and desert steppes in the Heihe River Basin.

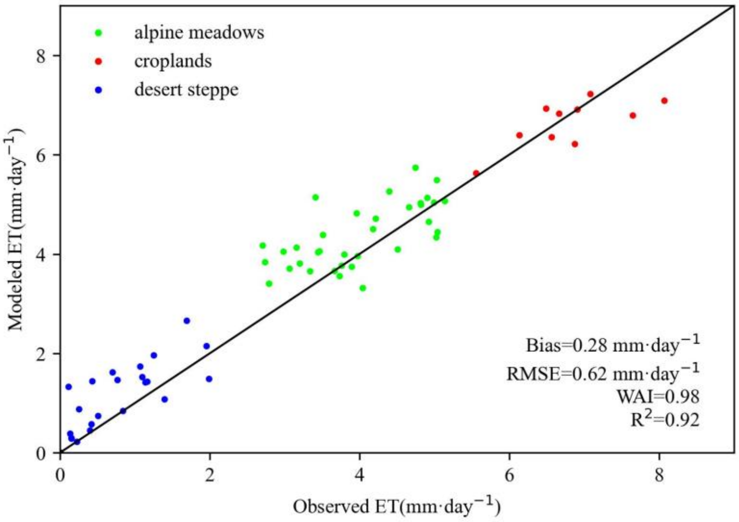

Figure 9. Scatterplot of observed daily ET from the EC systems and daily ET modeled via the $\text{TSEB}_{\text{SM+}}$ model at seven sites.

4. Discussion

4.1. Comparison of TSEB, $\text{TSEB}_{\text{SM,}}$ and $\text{TSEB}_{\text{SM+}}$ Models

The TSEB, $\text{TSEB}_{\text{SM,}}$ and $\text{TSEB}_{\text{SM+}}$ models have similar concepts according to the energy balance equation. However, the radiometric surface temperature is used in the TSEB model, which is applied as the model's boundary condition to separate the vegetation and soil temperatures, while the surface soil moisture is used in the TSEB_{SM} and $\text{TSEB}_{\text{SM+}}$ models instead of the radiometric surface temperature to avoid the lack of radiometric surface temperature observations obtained from remote sensing under cloudy conditions. In other words, the radiometric surface temperature is an input parameter that plays a key role in the relationship between the Ts and Tc for the TSEB model, while it is an output parameter for the TSEB_{SM} and $\text{TSEB}_{\text{SM+}}$ models.

The PT formulation is used in the TSEB_{SM} model to estimate the plant transpiration, which lacks sensitivity for the accommodation of varying vegetation stress levels [47] because canopy conductance controls the loss of water through transpiration and the uptake of carbon via photosynthesis and is also affected by soil water stress [73]. When the area was dry, the f_g and α_{PT} values were frequently low, making it challenging to distinguish the component temperatures from the radiometric surface temperature [35]. We incorporated the canopy conductance model, in which the effect of soil water stress was considered, into the TSEB_{SM} model instead of the PT formulation from the original model. The $\text{TSEB}_{\text{SM+}}$ model coupled the resistances from the soil and canopy to constrain the T and E components, which aligned more closely with the plant physiology and soil surface characteristics. Compared to the TSEB_{SM} model, such improvements not only improved the estimation accuracy for the $\text{TSEB}_{\text{SM+}}$ model under sparse vegetation cover or soil water stressed conditions, but also significantly improved the model's performance in dense vegetation cover or moist soil surface environments.

4.2. A Analysis of Model Performances Sensitivity to Soil Moisture

The soil moisture is one of the main input parameters for the $\text{TSEB}_{\text{SM+}}$ model. We first segmented the data from the three sites based on the soil moisture and assessed the LE estimation accuracy from the TSEB, $\text{TSEB}_{\text{SM,}}$ and $\text{TSEB}_{\text{SM+}}$ models for different intervals to analyze the model performance under different soil moisture conditions. The soil moisture was divided into five levels: <10%, 10–20%, 20–30%, 30–40%, and >40%. The LE errors from the three models for different intervals are shown in Figure 10.

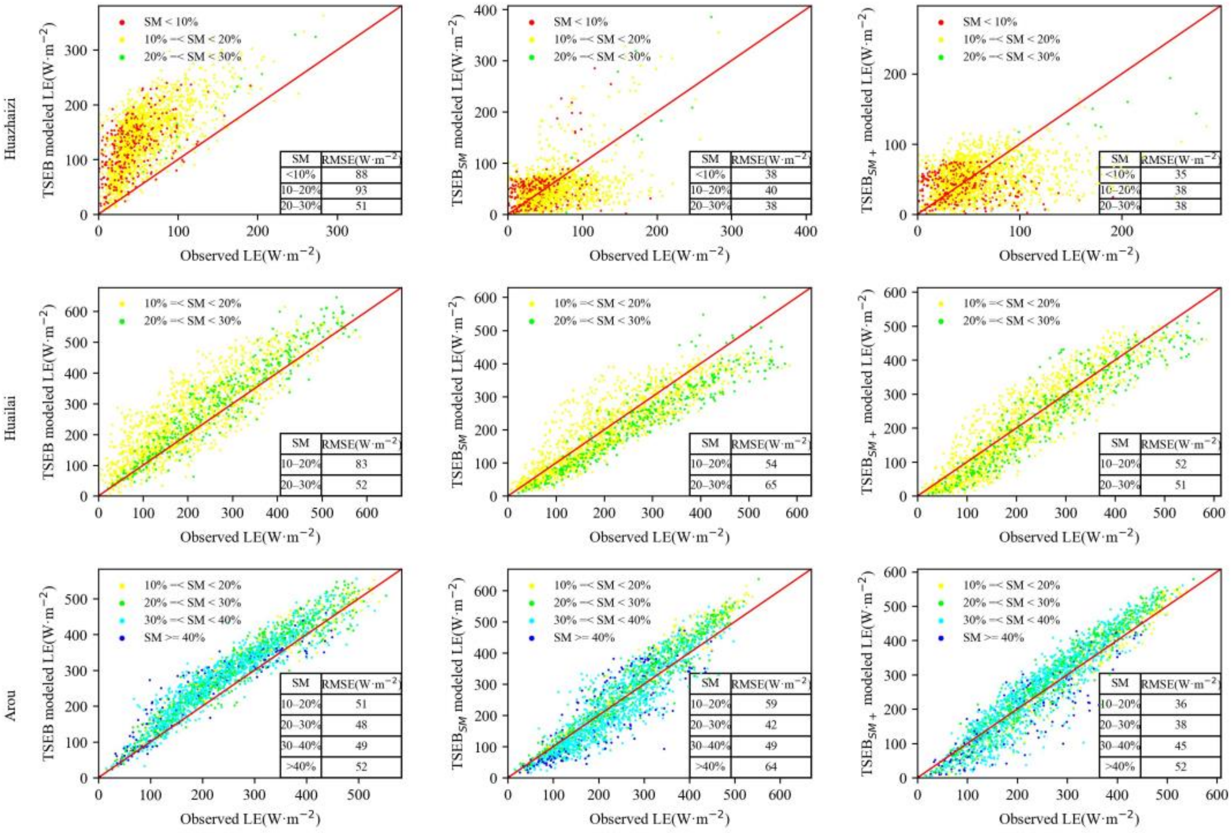

Figure 10. Scatterplots and tables of the comparison of the half-hour LE measured by the EC system and the estimation from the TSEB, TSEB$_{SM}$ and TSEB$_{SM+}$ models for the Huazhaizi, Huailai, and A'rou sites.

We found a good agreement when comparing the estimations via the TSEB and TSEB$_{SM}$ models with the observed LE for the Huazhaizi and Huailai sites, especially for the Huazhaizi site, where the soil moisture was almost below 20% during the study period. The TSEB$_{SM}$ model had a worse LE estimation when the soil moisture was in the range of 20–30%; however, the TSEB and TSEB$_{SM+}$ models had the opposite result. This is likely due to the higher LAI caused by the corn growing season, when the soil moisture was in the range of 20–30%. For the A'rou site, the LE RMSEs estimated via the TSEB$_{SM+}$ and TSEB models became similar with the increase in the soil moisture. The TSEB$_{SM+}$ model always had a better LE estimation performance than the TSEB model, and the TSEB model's performance became better with the increase in the soil moisture. In contrast, the LE estimation of the TSEB$_{SM}$ model was relatively poor, which may indicate that the TSEB$_{SM+}$ model has a better performance than the TSEB$_{SM}$ and TSEB models under high vegetation cover and water stress conditions.

To assess the sensitivity of the model to the soil moisture for different underlying surfaces, we also changed the soil moisture at intervals of 1% from 12% to 45% and analyzed the change in the LE. First, we ran the model with different soil moistures, which were used for the r_c or r_{ss} at the three sites, and then the different soil moistures which were used for the r_c and r_{ss} to run the model at the three sites (Figure 11).

The evaporation fraction (defined as the LE/(LE + H)) increased from 0.27 to 0.68 when modifying the soil moisture affecting the r_{ss} at the Huazhaizi site, which has low vegetation cover and where the soil evaporation constitutes the primary evapotranspiration component, while the fluctuation of the evaporation fraction remained relatively small when altering the soil moisture affecting the r_c. However, the evaporation fraction increased significantly from 0.39 to 0.82 and from 0.39 to 0.71 when modifying the soil moisture affecting the r_c at the Huailai and A'rou sites, which have high vegetation cover and where the plant transpiration is the main evapotranspiration component. In contrast, the increase in the soil moisture for the r_{ss} led to a relatively negligible change in the evaporation fraction. The relationship between the LE and soil moisture had a similar pattern to that observed for the evaporation fraction. Moreover, the variation in the LE at the Huailai site was greater than that at the A′rou site when the soil moisture affecting the r_{ss} was changed, which may be attributed to the higher LAI and larger contribution of T to the ET at the A′rou site. The findings suggest that soil moisture primarily regulates evapotranspiration by influencing the evaporation in areas with sparse vegetation and the transpiration in areas with dense vegetation.

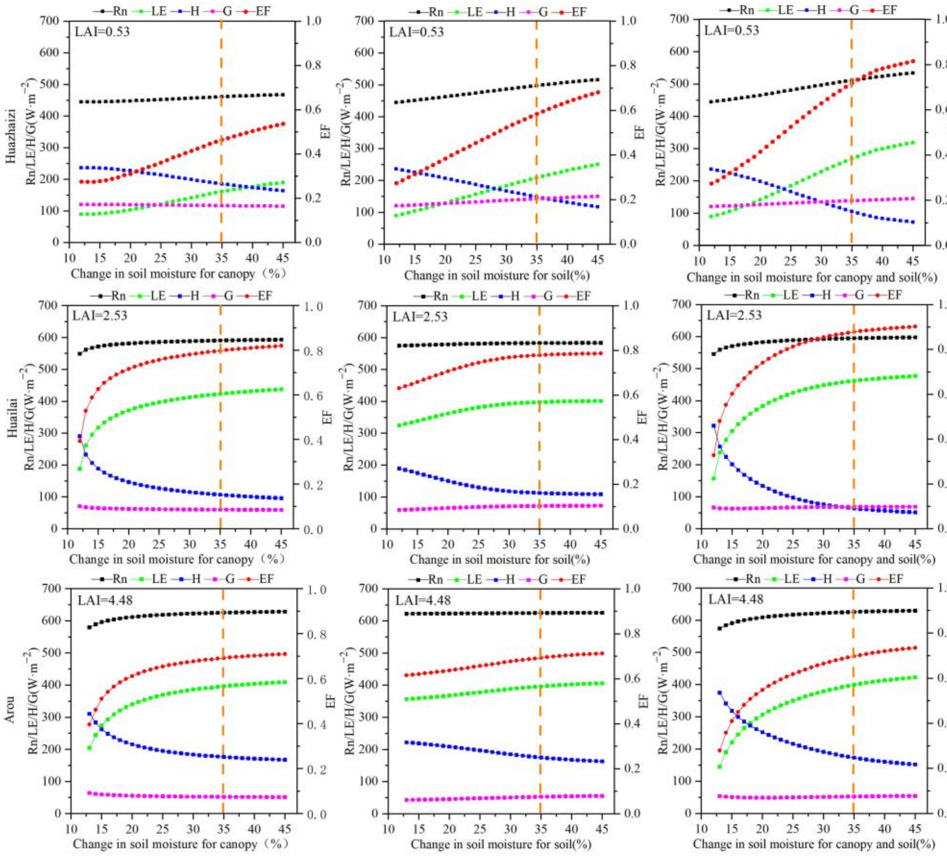

Figure 11. Energy fluxes and evaporation ratios from the $\text{TSEB}_{\text{SM+}}$ model with a change in the soil moisture range from 12 to 45% for the Huazhaizi, Huailai and A′rou sites. The orange dotted line indicates that the LE growth rate estimated via the model decreases significantly when the soil moisture is exceeded.

Obvious positive LE and evaporation fraction trends were observed when altering the soil moisture which simultaneously constrained the r_c and r_{ss}. This is likely because both the soil surface and canopy resistances diminish with the increase in the soil moisture, which weakens the influence on the evapotranspiration. However, the evaporation fraction has an approximately liner relationship with the soil moisture at the Huazhaizi site, while the growth rate for the evaporation fraction slowed down with the increase in the soil moisture at the Huailai and A′rou sites. This may indicate that the vegetation has an effect on the ET and usually rapidly reduces the impact with the increase in the soil moisture in high vegetation cover conditions; however, this effect exists persistently under sparse vegetation cover conditions until the soil is saturated. The evaporation fraction gradually increased at each site, but the growth rate slowed or even plateaued with the increase in the soil moisture. When the soil moisture exceeded 35%, the evaporation fraction was basically stable for the Huailai and A′rou sites and slowly increased for the Huazhaizi site. The soil moisture may no longer act as a limiting factor for evapotranspiration once it reaches saturation.

5. Conclusions

In this study, the Jarvis canopy resistance, for which the influence of the soil moisture on the canopy conductance was considered, was coupled to the $TSEB_{SM}$ model as substitute for the PT approximation for plant transpiration, and the new $TSEB_{SM+}$ model was developed to estimate the ET. The model was assessed at the Huazhaizi, Huailai, and A'rou sites with different underlying surfaces and was compared with the $TSEB_{SM}$ and original TSEB models. The $TSEB_{SM+}$ model exhibited a notable improvement for the flux/ET estimation in arid and semi-arid regions. It showed better performance than the TSEB model under soil water stressed conditions and better performance than the $TSEB_{SM}$ model under high vegetation cover conditions. Moreover, the daily changes in the ET estimated via the $TSEB_{SM+}$ model have trends that are more similar to those of the EC measurements than the ET predicted via the $TSEB_{SM}$ and TSEB models. The $TSEB_{SM+}$ model could also be effectively applied to the estimation of the daily ET at the regional scale in arid and semi-arid regions. Finally, the $TSEB_{SM+}$ model is sensitive to soil moisture, and its performance improves as the soil moisture decreases. Overall, the $TSEB_{SM+}$ model exhibited commendable performance for the cropland with corn, desert steppe, and alpine meadow environments. Therefore, when combined with vegetation cover and surface soil moisture data, the $TSEB_{SM+}$ model is potentially a more effective tool for monitoring the ET in arid and semi-arid regions. Nonetheless, further validation across diverse landcover types at flux observation sites is necessary to ascertain its applicability as a conventional method. However, the absence of parameters that are sensitive to precipitation in the model resulted in a significant underestimation of the LE during precipitation events. Additionally, the model primarily relies on soil moisture that can be obtained via microwave satellites, and the availability of high-resolution soil moisture products enables the $TSEB_{SM+}$ model to estimate the daily ET at a more detailed regional scale.

Author Contributions: Conceptualization, Q.Z. and J.K.; methodology, Q.Z. and J.K.; software, Q.Z., L.W. and X.W.; validation, Q.Z., J.K. and X.W.; formal analysis, Q.Z., J.K. and L.W.; investigation, Q.Z., L.W., X.W., Y.J. and Y.Z.; resources, J.K.; data curation, X.W., Y.J. and Y.Z.; writing—original draft preparation, Q.Z.; writing—review and editing, J.K. and Z.Z.; visualization, Q.Z., L.W. and X.W.; supervision, J.K. and Z.Z.; project administration, J.K.; funding acquisition, J.K. All authors have read and agreed to the published version of the manuscript.

Funding: This work was supported by the National Natural Science Foundation of China (No. 42071345).

Institutional Review Board Statement: Not applicable.

Data Availability Statement: The LAI products were provided by Global Land Surface Satellite products (http://www.glass.umd.edu/LAI/, accessed on 19 December 2024). The soil moisture, meteorological data, land surface temperature, and site data (including the automatic weather station and the eddy covariance system) for the Heihe River Basin were provided by the National Tibetan Plateau Data Center (https://www.tpdc.ac.cn/en/, accessed on 19 December 2024).

Acknowledgments: We thank all the scientists, engineers, and students who participated in the field campaigns, and we appreciate all the reviewers and editors for their comments on this paper.

Conflicts of Interest: The authors declare no conflicts of interest.

References

1. Jung, M.; Reichstein, M.; Ciais, P.; Seneviratne, S.I.; Sheffield, J.; Goulden, M.L.; Bonan, G.; Cescatti, A.; Chen, J.; de Jeu, R.; et al. Recent Decline in the Global Land Evapotranspiration Trend due to Limited Moisture Supply. *Nature* **2010**, *467*, 951–954. [CrossRef] [PubMed]
2. Zhang, K.; Kimball, J.S.; Running, S.W. A Review of Remote Sensing Based Actual Evapotranspiration Estimation. *WIREs Water* **2016**, *3*, 834–853. [CrossRef]

3. Trenberth, K.E.; Smith, L.; Qian, T.; Dai, A.; Fasullo, J. Estimates of the Global Water Budget and Its Annual Cycle Using Observational and Model Data. *J. Hydrometeorol.* **2007**, *8*, 758–769. [CrossRef]
4. Trenberth, K.E.; Fasullo, J.T.; Kiehl, J. Earth's Global Energy Budget. *Bull. Am. Meteorol. Soc.* **2009**, *90*, 311–324. [CrossRef]
5. García, M.; Sandholt, I.; Ceccato, P.; Ridler, M.; Mougin, E.; Kergoat, L.; Morillas, L.; Timouk, F.; Fensholt, R.; Domingo, F. Actual Evapotranspiration in Drylands Derived from In-Situ and Satellite Data: Assessing Biophysical Constraints. *Remote Sens. Environ.* **2013**, *131*, 103–118. [CrossRef]
6. Wang, K.; Dickinson, R.E. A Review of Global Terrestrial Evapotranspiration: Observation, Modeling, Climatology, and Climatic Variability. *Rev. Geophys.* **2012**, *50*, 2. [CrossRef]
7. Rango, A. Application of Remote Sensing Methods to Hydrology and Water Resources. *Hydrol. Sci. J.* **1994**, *39*, 309–320. [CrossRef]
8. Kustas, W.P.; Norman, J.M. Evaluation of Soil and Vegetation Heat Flux Predictions Using a Simple Two-Source Model with Radiometric Temperatures for Partial Canopy Cover. *Agric. For. Meteorol.* **1999**, *94*, 13–29. [CrossRef]
9. Tang, R.; Li, Z.-L. An End-Member-Based Two-Source Approach for Estimating Land Surface Evapotranspiration from Remote Sensing Data. *IEEE Trans. Geosci. Remote Sens.* **2017**, *55*, 5818–5832. [CrossRef]
10. Liao, Q.-Y.; Leng, P.; Ren, C.; Li, Z.-L.; Gao, M.-F.; Duan, S.-B.; Zhang, X.; Shang, G.-F. Evapotranspiration Retrieval under Different Aridity Conditions over North American Grasslands. *IEEE Trans. Geosci. Remote Sens.* **2020**, *58*, 7205–7215. [CrossRef]
11. Su, Z. The Surface Energy Balance System (SEBS) for Estimation of Turbulent Heat Fluxes. *Hydrol. Earth Syst. Sci.* **2002**, *6*, 85–100. [CrossRef]
12. Norman, J.M.; Kustas, W.P.; Humes, K.S. Source Approach for Estimating Soil and Vegetation Energy Fluxes in Observations of Directional Radiometric Surface Temperature. *Agric. For. Meteorol.* **1995**, *77*, 263–293. [CrossRef]
13. Fisher, J.B.; Tu, K.P.; Baldocchi, D.D. Global Estimates of the Land–Atmosphere Water Flux Based on Monthly AVHRR and ISLSCP-II Data, Validated at 16 FLUXNET Sites. *Remote Sens. Environ.* **2008**, *112*, 901–919. [CrossRef]
14. Li, X.; Kang, S.; Li, F.; Jiang, X.; Tong, L.; Ding, R.; Li, S.; Du, T. Applying Segmented Jarvis Canopy Resistance into Penman-Monteith Model Improves the Accuracy of Estimated Evapotranspiration in Maize for Seed Production with Film-Mulching in Arid Area. *Agric. Water Manag.* **2016**, *178*, 314–324. [CrossRef]
15. Fang, S.-L.; Lin, Y.-S.; Chang, S.-C.; Chang, Y.-L.; Tsai, B.-Y.; Kuo, B.-J. Using Artificial Intelligence Algorithms to Estimate and Short-Term Forecast the Daily Reference Evapotranspiration with Limited Meteorological Variables. *Agriculture* **2024**, *14*, 510. [CrossRef]
16. Cui, Y.; Jia, L. Estimation of Evapotranspiration of "Soil-Vegetation" System with a Scheme Combining a Dual-Source Model and Satellite Data Assimilation. *J. Hydrol.* **2021**, *603*, 127145. [CrossRef]
17. Elbeltagi, A.; Srivastava, A.; Li, P.; Jiang, J.; Deng, J.; Rajput, J.; Khadke, L.; Awad, A. Forecasting Actual Evapotranspiration without Climate Data Based on Stacked Integration of DNN and Meta-Heuristic Models across China from 1958 to 2021. *J. Environ. Manag.* **2023**, *345*, 118697. [CrossRef]
18. Rajput, J.; Singh, M.; Lal, K.; Khanna, M.; Sarangi, A.; Mukherjee, J.; Singh, S. Data-Driven Reference Evapotranspiration (ET0) Estimation: A Comparative Study of Regression and Machine Learning Techniques. *Environ. Dev. Sustain.* **2023**, *26*, 12679–12706. [CrossRef]
19. Rajput, J.; Singh, M.; Lal, K.; Khanna, M.; Sarangi, A.; Mukherjee, J.; Singh, S. Assessment of data intelligence algorithms in modeling daily reference evapotranspiration under input data limitation scenarios in semi-arid climatic condition. *Water Sci. Technol.* **2023**, *87*, 2504–2528. [CrossRef]
20. Rajput, J.; Singh, M.; Lal, K.; Khanna, M.; Sarangi, A.; Mukherjee, J.; Singh, S. Selection of Alternate Reference Evapotranspiration Models Based on Multi-Criteria Decision Ranking for Semiarid Climate. *Environ. Dev. Sustain.* **2023**, *26*, 11171–11216. [CrossRef]
21. Kustas, W.; Anderson, M. Advances in Thermal Infrared Remote Sensing for Land Surface Modeling. *Agric. For. Meteorol.* **2009**, *149*, 2071–2081. [CrossRef]
22. Liou, Y.-A.; Kar, S. Evapotranspiration Estimation with Remote Sensing and Various Surface Energy Balance Algorithms—A Review. *Energies* **2014**, *7*, 2821–2849. [CrossRef]
23. Anderson, M. A Two-Source Time-Integrated Model for Estimating Surface Fluxes Using Thermal Infrared Remote Sensing. *Remote Sens. Environ.* **1997**, *60*, 195–216. [CrossRef]
24. Colaizzi, P.D.; Evett, S.R.; Howell, T.A.; Gowda, P.H.; O'Shaughnessy, S.A.; Tolk, J.A.; Kustas, W.P.; Anderson, M.C. Two-Source Energy Balance Model: Refinements and Lysimeter Tests in the Southern High Plains. *Trans. ASABE* **2012**, *55*, 551–562. [CrossRef]
25. Kustas, W.P.; Norman, J.M. A Two-Source Energy Balance Approach Using Directional Radiometric Temperature Observations for Sparse Canopy Covered Surfaces. *Agron. J.* **2000**, *92*, 847–854. [CrossRef]
26. Bastiaanssen, W.G.M.; Menenti, M.; Feddes, R.A.; Holtslag, A.A.M. A Remote Sensing Surface Energy Balance Algorithm for Land (SEBAL). 1. Formulation. *J. Hydrol.* **1998**, *212–213*, 198–212. [CrossRef]
27. Tang, R.; Li, Z.-L.; Jia, Y.; Li, C.; Sun, X.; Kustas, W.P.; Anderson, M.C. An Intercomparison of Three Remote Sensing-Based Energy Balance Models Using Large Aperture Scintillometer Measurements over a Wheat–Corn Production Region. *Remote Sens. Environ.* **2011**, *115*, 3187–3202. [CrossRef]
28. Yao, W.; Han, M.; Xu, S. Estimating the Regional Evapotranspiration in Zhalong Wetland with the Two-Source Energy Balance (TSEB) Model and Landsat7/ETM+ Images. *Ecol. Inform.* **2010**, *5*, 348–358. [CrossRef]
29. French, A.N.; Hunsaker, D.J.; Thorp, K.R. Remote Sensing of Evapotranspiration over Cotton Using the TSEB and METRIC Energy Balance Models. *Remote Sens. Environ.* **2015**, *158*, 281–294. [CrossRef]

30. Timmermans, W.J.; Kustas, W.P.; Anderson, M.C.; French, A.N. An Intercomparison of the Surface Energy Balance Algorithm for Land (SEBAL) and the Two-Source Energy Balance (TSEB) Modeling Schemes. *Remote Sens. Environ.* **2007**, *108*, 369–384. [CrossRef]
31. Gao, Y.; Long, D. Intercomparison of Remote Sensing-Based Models for Estimation of Evapotranspiration and Accuracy Assessment Based on SWAT. *Hydrol. Process.* **2008**, *22*, 4850–4869. [CrossRef]
32. Kustas, W.P.; Bindlish, R.; French, A.N.; Schmugge, T.J. Comparison of Energy Balance Modeling Schemes Using Microwave-Derived Soil Moisture and Radiometric Surface Temperature. *Water Resour. Res.* **2003**, *39*, 2. [CrossRef]
33. Morillas, L.; García, M.E.; Nieto, H.; Villagarcía, L.; Sandholt, I.; González-Dugo, M.P.; Zarco-Tejada, P.J.; Domingo, F. Using Radiometric Surface Temperature for Surface Energy Flux Estimation in Mediterranean Drylands from a Two-Source Perspective. *Remote Sens. Environ.* **2013**, *136*, 234–246. [CrossRef]
34. Morillas, L.; Villagarcía, L.; Domingo, F.; Nieto, H.; Uclés, O.; García, M. Environmental Factors Affecting the Accuracy of Surface Fluxes from a Two-Source Model in Mediterranean Drylands: Upscaling Instantaneous to Daytime Estimates. *Agric. For. Meteorol.* **2014**, *189–190*, 140–158. [CrossRef]
35. Kustas, W.P.; Nieto, H.; Morillas, L.; Anderson, M.C.; Alfieri, J.G.; Hipps, L.E.; Villagarcía, L.; Domingo, F.; Garcia, M. Revisiting the Paper "Using Radiometric Surface Temperature for Surface Energy Flux Estimation in Mediterranean Drylands from a Two-Source Perspective". *Remote Sens. Environ.* **2016**, *184*, 645–653. [CrossRef]
36. Li, Y.; Kustas, W.P.; Huang, C.; Nieto, H.; Haghighi, E.; Anderson, M.C.; Domingo, F.; García, M.; Scott, R.L. Evaluating Soil Resistance Formulations in Thermal-Based Two-Source Energy Balance (TSEB) Model: Implications for Heterogeneous Semiarid and Arid Regions. *Water Resour. Res.* **2019**, *55*, 1059–1078. [CrossRef]
37. Feng, J.; Wang, W.; Che, T.; Xu, F. Performance of the Improved Two-Source Energy Balance Model for Estimating Evapotranspiration over the Heterogeneous Surface. *Agric. Water Manag.* **2023**, *278*, 108159. [CrossRef]
38. Kustas, W.P.; Zhan, X.; Schmugge, T.J. Combining Optical and Microwave Remote Sensing for Mapping Energy Fluxes in a Semiarid Watershed. *Remote Sens. Environ.* **1998**, *64*, 116–131. [CrossRef]
39. Chanzy, A.; Bruckler, L. Significance of Soil Surface Moisture with Respect to Daily Bare Soil Evaporation. *Water Resour. Res.* **1993**, *29*, 1113–1125. [CrossRef]
40. Wang, Y.; Zhang, Y.; Yu, X.; Jia, G.; Liu, Z.; Sun, L.; Zheng, P.; Zhu, X. Grassland Soil Moisture Fluctuation and Its Relationship with Evapotranspiration. *Ecol. Indic.* **2021**, *131*, 108196. [CrossRef]
41. Gokmen, M.; Vekerdy, Z.; Verhoef, A.; Verhoef, W.; Batelaan, O.; van der Tol, C. Integration of Soil Moisture in SEBS for Improving Evapotranspiration Estimation under Water Stress Conditions. *Remote Sens. Environ.* **2012**, *121*, 261–274. [CrossRef]
42. Purdy, A.J.; Fisher, J.B.; Goulden, M.L.; Colliander, A.; Halverson, G.R.; Tu, K.P.; Famiglietti, J.S. SMAP Soil Moisture Improves Global Evapotranspiration. *Remote Sens. Environ.* **2018**, *219*, 1–14. [CrossRef]
43. Elfarkh, J.; Er-Raki, S.; Ezzahar, J.; Chehbouni, A.; Aithssaine, B.; Amazirh, A.; Khabba, S.; Jarlan, L. Integrating Thermal Stress Indexes within Shuttleworth–Wallace Model for Evapotranspiration Mapping over a Complex Surface. *Irrig. Sci.* **2020**, *39*, 45–61. [CrossRef]
44. Kustas, W.P.; Zhan, X.; Jackson, T.J. Mapping Surface Energy Flux Partitioning at Large Scales with Optical and Microwave Remote Sensing Data from Washita '92. *Water Resour. Res.* **1999**, *35*, 265–277. [CrossRef]
45. Kustas, W.P.; Jackson, T.J.; French, A.N.; MacPherson, J.I. Verification of Patch- and Regional-Scale Energy Balance Estimates Derived from Microwave and Optical Remote Sensing during SGP97. *J. Hydrometeorol.* **2001**, *2*, 254–273. [CrossRef]
46. Sellers, P.J.; Heiser, M.D.; Hall, F.G. Relations between Surface Conductance and Spectral Vegetation Indices at Intermediate (100 m^2 to 15 km^2) Length Scales. *J. Geophys. Res.* **1992**, *97*, 19033. [CrossRef]
47. Li, F.; Kustas, W.P.; Anderson, M.C.; Jackson, T.J.; Bindlish, R.; Prueger, J.H. Comparing the Utility of Microwave and Thermal Remote-Sensing Constraints in Two-Source Energy Balance Modeling over an Agricultural Landscape. *Remote Sens. Environ.* **2006**, *101*, 315–328. [CrossRef]
48. Gan, G.; Gao, Y. Estimating Time Series of Land Surface Energy Fluxes Using Optimized Two Source Energy Balance Schemes: Model Formulation, Calibration, and Validation. *Agric. For. Meteorol.* **2015**, *208*, 62–75. [CrossRef]
49. Ait Hssaine, B.; Merlin, O.; Rafi, Z.; Ezzahar, J.; Jarlan, L.; Khabba, S.; Er-Raki, S. Calibrating an Evapotranspiration Model Using Radiometric Surface Temperature, Vegetation Cover Fraction and Near-Surface Soil Moisture Data. *Agric. For. Meteorol.* **2018**, *256–257*, 104–115. [CrossRef]
50. Song, L.; Kustas, W.P.; Liu, S.; Colaizzi, P.D.; Nieto, H.; Xu, Z.; Ma, Y.; Li, M.; Xu, T.; Agam, N.; et al. Applications of a Thermal-Based Two-Source Energy Balance Model Using Priestley-Taylor Approach for Surface Temperature Partitioning under Advective Conditions. *J. Hydrol.* **2016**, *540*, 574–587. [CrossRef]
51. Song, L.; Ding, Z.; Kustas, W.P.; Xu, Y.; Zhao, G.; Liu, S.; Ma, M.; Xue, K.; Bai, Y.; Xu, Z. Applications of a Thermal-Based Two-Source Energy Balance Model Coupled to Surface Soil Moisture. *Remote Sens. Environ.* **2022**, *271*, 112923. [CrossRef]
52. Ait Hssaine, B.; Merlin, O.; Ezzahar, J.; Ojha, N.; Er-Raki, S.; Khabba, S. An Evapotranspiration Model Self-Calibrated from Remotely Sensed Surface Soil Moisture, Land Surface Temperature and Vegetation Cover Fraction: Application to Disaggregated SMOS and MODIS Data. *Hydrol. Earth Syst. Sci.* **2020**, *24*, 1781–1803. [CrossRef]
53. Ait Hssaine, B.; Chehbouni, A.; Er-Raki, S.; Khabba, S.; Ezzahar, J.; Ouaadi, N.; Ojha, N.; Rivalland, V.; Merlin, O. On the Utility of High-Resolution Soil Moisture Data for Better Constraining Thermal-Based Energy Balance over Three Semi-Arid Agricultural Areas. *Remote Sens.* **2021**, *13*, 727. [CrossRef]

54. Zhuang, Q.; Wu, B. Estimating Evapotranspiration from an Improved Two-Source Energy Balance Model Using ASTER Satellite Imagery. *Water* **2015**, *7*, 6673–6688. [CrossRef]
55. Tao, S.; Song, L.; Zhao, G.; Zhao, L. Simulation and Assessment of Daily Evapotranspiration in the Heihe River Basin over a Long Time Series Based on TSEB-SM. *Remote Sens.* **2024**, *16*, 462. [CrossRef]
56. Gan, G.; Kang, T.; Yang, S.; Bu, J.; Feng, Z.; Gao, Y. An Optimized Two Source Energy Balance Model Based on Complementary Concept and Canopy Conductance. *Remote Sens. Environ.* **2019**, *223*, 243–256. [CrossRef]
57. Bu, J.; Gan, G.; Chen, J.; Su, Y.; García, M.; Gao, Y. Biophysical Constraints on Evapotranspiration Partitioning for a Conductance-Based Two Source Energy Balance Model. *J. Hydrol.* **2021**, *603*, 127179. [CrossRef]
58. Yu, M.-H.; Ding, G.-D.; Gao, G.-L.; Zhao, Y.-Y.; Yan, L.; Sai, K. Using Plant Temperature to Evaluate the Response of Stomatal Conductance to Soil Moisture Deficit. *Forests* **2015**, *6*, 3748–3762. [CrossRef]
59. Jarvis, P.G. The Interpretation of the Variation in Leaf Water Potential and Stomatal Conductance Found in Canopies in the Field. *Philos. Trans. R. Soc. Lond. B Biol. Sci.* **1976**, *273*, 593–610. [CrossRef]
60. Stewart, J.B. Modelling Surface Conductance of Pine Forest. *Agric. For. Meteorol.* **1988**, *43*, 19–35. [CrossRef]
61. Liu, S.M.; Xu, Z.W.; Zhu, Z.L.; Jia, Z.Z.; Zhu, M.J. Measurements of Evapotranspiration from Eddy-Covariance Systems and Large Aperture Scintillometers in the Hai River Basin, China. *J. Hydrol.* **2013**, *487*, 24–38. [CrossRef]
62. Liu, S.; Li, X.; Xu, Z.; Che, T.; Xiao, Q.; Ma, M.-G.; Liu, Q.; Jin, R.; Guo, J.; Wang, L.; et al. The Heihe Integrated Observatory Network: A Basin-Scale Land Surface Processes Observatory in China. *Vadose Zone J.* **2018**, *17*, 1–21. [CrossRef]
63. Twine, T.E.; Kustas, W.P.; Norman, J.M.; Cook, D.R.; Houser, P.R.; Meyers, T.P.; Prueger, J.H.; Starks, P.J.; Wesely, M.L. Correcting Eddy-Covariance Flux Underestimates over a Grassland. *Agric. For. Meteorol.* **2000**, *103*, 279–300. [CrossRef]
64. Pan, X.; Li, X.; Shi, X.; Han, X.; Luo, L.; Wang, L. Dynamic Downscaling of Near-Surface Air Temperature at the Basin Scale Using WRF—A Case Study in the Heihe River Basin, China. *Front. Earth Sci.* **2012**, *6*, 314–323. [CrossRef]
65. Zheng, C.; Jia, L.; Zhao, T. A 21-Year Dataset (2000–2020) of Gap-Free Global Daily Surface Soil Moisture at 1-km Grid Resolution. *Sci. Data* **2023**, *10*, 139. [CrossRef]
66. Tang, W.; Zhou, J.; Ma, J.; Wang, Z.; Ding, L.; Zhang, X.; Zhang, X. TRIMS LST: A Daily 1 km All-Weather Land Surface Temperature Dataset for China's Landmass and Surrounding Areas (2000–2022). *Earth Syst. Sci. Data* **2024**, *16*, 387–419. [CrossRef]
67. Kustas, W.P.; Daughtry, C.S.T. Estimation of the Soil Heat Flux/Net Radiation Ratio from Spectral Data. *Agric. For. Meteorol.* **1990**, *49*, 205–223. [CrossRef]
68. Camillo, P.J.; Gurney, R.J. A resistance parameter for bare-soil evaporation models. *Soil Sci.* **1986**, *141*, 95–105. [CrossRef]
69. Long, D.; Singh, V.P. A Two-Source Trapezoid Model for Evapotranspiration (TTME) from Satellite Imagery. *Remote Sens. Environ.* **2012**, *121*, 370–388. [CrossRef]
70. Liu, X.; Xu, J.; Wang, W.; Lv, Y.; Li, Y. Modeling Rice Evapotranspiration under Water-Saving Irrigation Condition: Improved Canopy-Resistance-Based. *J. Hydrol.* **2020**, *590*, 125435. [CrossRef]
71. Xu, J.; Liu, X.; Yang, S.; Qi, Z.; Wang, Y. Modeling Rice Evapotranspiration under Water-Saving Irrigation by Calibrating Canopy Resistance Model Parameters in the Penman-Monteith Equation. *Agric. Water Manag.* **2017**, *182*, 55–66. [CrossRef]
72. Song, W.-K.; Cui, Y.-J.; Ye, W.-M. Modelling of Water Evaporation from Bare Sand. *Eng. Geol.* **2018**, *233*, 281–289. [CrossRef]
73. Bu, J.; Gan, G.; Chen, J.; Su, Y.; Yuan, M.; Gao, Y.; Domingo, F.; López-Ballesteros, A.; Migliavacca, M.; El-Madany, T.S.; et al. Dryland Evapotranspiration from Remote Sensing Solar-Induced Chlorophyll Fluorescence: Constraining an Optimal Stomatal Model within a Two-Source Energy Balance Model. *Remote Sens. Environ.* **2024**, *303*, 113999. [CrossRef]

Disclaimer/Publisher's Note: The statements, opinions and data contained in all publications are solely those of the individual author(s) and contributor(s) and not of MDPI and/or the editor(s). MDPI and/or the editor(s) disclaim responsibility for any injury to people or property resulting from any ideas, methods, instructions or products referred to in the content.